Chinese Physics B

PAPER

Realization of low-energy type-II Dirac fermions in $(Ir_{1-x}Pt_x)Te_2$ superconductors*

To cite this article: Bin-Bin Fu *et al* 2019 *Chinese Phys. B* **28** 037103

RAPID COMMUNICATION

Realization of low-energy type-II Dirac fermions in $(Ir_{1-x}Pt_x)Te_2$ superconductors*

Bin-Bin Fu(付彬彬)[1,2,†], Chang-Jiang Yi(伊长江)[1,2,†], Zhi-Jun Wang(王志俊)[1,†], Meng Yang(杨萌)[1,2], Bai-Qing Lv(吕佰晴)[1,2], Xin Gao(高鑫)[1,2], Man Li(李满)[3,4], Yao-Bo Huang(黄耀波)[3], Hong-Ming Weng(翁红明)[1,5], You-Guo Shi(石友国)[1,5,‡], Tian Qian(钱天)[1,5,6,§], and Hong Ding(丁洪)[1,6,¶]

[1] *Beijing National Laboratory for Condensed Matter Physics and Institute of Physics, Chinese Academy of Sciences, Beijing* 100190, *China*
[2] *University of Chinese Academy of Sciences, Beijing* 100049, *China*
[3] *Shanghai Synchrotron Radiation Facility, Shanghai Institute of Applied Physics, Chinese Academy of Sciences, Shanghai* 201204, *China*
[4] *Department of Physics and Beijing Key Laboratory of Opto-electronic Functional Materials & Micro-nano Devices, Renmin University of China, Beijing* 100872, *China*
[5] *Songshan Lake Materials Laboratory, Dongguan* 523808, *China*
[6] *CAS Center for Excellence in Topological Quantum Computation, University of Chinese Academy of Sciences, Beijing* 100190, *China*

(Received 12 January 2019; revised manuscript received 30 January 2019; published online 22 February 2019)

Topological Dirac semimetals (DSMs) present a kind of topologically nontrivial quantum state of matter, which has massless Dirac fermions in the bulk and topologically protected states on certain surfaces. In superconducting DSMs, the effects of their nontrivial topology on superconducting pairing could realize topological superconductivity in the bulk or on the surface. As superconducting pairing takes place at the Fermi level E_F, to make the effects possible, the Dirac points should lie in the vicinity of E_F so that the topological electronic states can participate in the superconducting paring. Here, we show using angle-resolved photoelectron spectroscopy that in a series of $(Ir_{1-x}Pt_x)Te_2$ compounds, the type-II Dirac points reside around E_F in the superconducting region, in which the bulk superconductivity has a maximum T_c of ~ 3 K. The realization of the coexistence of bulk superconductivity and low-energy Dirac fermions in $(Ir_{1-x}Pt_x)Te_2$ paves the way for studying the effects of the nontrivial topology in DSMs on the superconducting state.

Keywords: type-II Dirac semimetal, superconductor, topological superconducting, angle-resolved photoemission spectroscopy (ARPES), substitution

PACS: 71.20.–b, 79.60.–i, 73.20.At, 74.70.–b **DOI:** 10.1088/1674-1056/28/3/037103

The interplay between topological states and superconductivity is an important issue in condensed matter physics.[1,2] One consequence of the interplay is the generation of Majorana fermions at the boundary of a topological superconductor, which can be used for topological quantum computation. Tremendous efforts have been made to induce superconductivity in topological materials through various approaches, such as introducing carriers, applying external pressure, and proximity effect, or to search for superconductors with nontrivial topological electronic states. Superconductivity has been observed in doped topological insulators, such as Cu-intercalated Bi_2Se_3,[3] Bi_2Te_3 under pressure,[4] Bi_2Se_3 thin films on superconducting $NbSe_2$ substrate,[5] and In-doped SnTe.[6] Several superconductors such as *R*PtBi (*R*: rare earth elements),[7–10] Bi_2Pd,[11] and $FeTe_{0.55}Se_{0.45}$[12,13] have been revealed to have a nontrivial topology similar to that of topological insulators.

In addition to superconducting topological insulators, theory has proposed that in superconducting Dirac and Weyl semimetals, topological superconductivity can also be realized for the bulk or the surface due to their nontrivial topology.[14–16] Experimentally, the superconductivity was induced by point contact[17,18] or under high pressure[19] in the Dirac semimetal (DSM) Cd_3As_2. The point contact spectra of Cd_3As_2 show a zero-bias conductance peak, suggesting unconventional superconductivity around the point contact region.[17,18] Recent studies have reported that several transition metal dichalcogenide (TMD) compounds $PtTe_2$,[20] $PdTe_2$,[21,22] and $PtSe_2$[23] with the CdI_2-type 1T structure host type-II Dirac points in their electronic structures. As illustrated in Figs. 1(c) and 1(d), distinct from type-I DSMs like Na_3Bi[24,25] and Cd_3As_2,[26,27] type-II DSMs possess over-

*Project supported by the Ministry of Science and Technology of China (Grant Nos. 2016YFA0300600, 2016YFA0401000, 2016YFA0302400, and 2017YFA0302901), the National Natural Science Foundation of China (Grant Nos. 11622435, U1832202, and 11674369), the Chinese Academy of Sciences (Grant Nos. QYZDB-SSW-SLH043, XDB07000000, and XDPB08-1), and the Beijing Municipal Science and Technology Commission, China (Grant No. Z171100002017018).

†These authors contributed equally to this work.
‡Corresponding author. E-mail: ygshi@iphy.ac.cn
§Corresponding author. E-mail: tqian@iphy.ac.cn
¶Corresponding author. E-mail: dingh@iphy.ac.cn

tilted Dirac cones so that the two Dirac bands have the same sign in their slope along one direction, in analogy to the type-II Weyl semimetals.[28–30] As the type-II Dirac points in these TMD compounds reside far below E_F, the Dirac fermions should have little contribution to the low-energy quasiparticle excitations at E_F. Very recently, Fei *et al.* reported that the energy position of the type-II Dirac points in $Ir_{1-x}Pt_xTe_2$ can be easily tuned by element substitution.[31] The Dirac points arrive at E_F at $x \sim 0.3$, where a bulk superconductivity emerges with $T_c = 0.15$ K.

In this work, by combining angle-resolved photoemission spectroscopy (ARPES), energy-dispersive x-ray spectroscopy (EDX), x-ray diffraction (XRD), and transport measurements, we systematically investigated the evolution of electronic structures and superconductivity of $(Ir_{1-x}Pt_x)Te_2$ with different doping levels. We found that the type-II Dirac points lie around E_F in the superconducting region, in which the bulk superconductivity has a maximum T_c of ~ 3 K, which is accessible in many experimental techniques, making it possible to study the physical properties of Dirac fermions in the superconducting state.

High quality $(Ir_{1-x}Pt_x)Te_2$ single crystals were synthesized by Te flux method. The chemical compositions of the single crystals for each doping level were analyzed by EDX in a Hitachi S-4800 at an accelerating voltage of 15 keV. Longitudinal resistivity was measured in an Oxford He-3. High resolution ARPES measurements were performed at the "Dreamline" beamline of the Shanghai Synchrotron Radiation Facility, the I05 beamline of the Diamond Light Source, and the 13U beamline of the National Synchrotron Radiation Laboratory at Hefei, with the energy and angular resolutions set at 15 meV and 0.2°, respectively. All the samples were cleaved *in situ* in vacuum condition better than 5×10^{-11} Torr and measured between 15–20 K. The first-principles calculations were performed to calculate the electronic structure of the 1T-structure $IrTe_2$ with the projector augmented wave (PAW) method as implemented in VASP package.[32] The tight-binding Hamiltonians of semi-infinite samples are constructed by the maximally localized Wannier functions (MLWFs) for all the Ir d and Te p orbitals, which are generated from the first-principles calculations. The (100) surface Green's functions of the semi-infinite sample are obtained using an iterative method.

Our first-principles calculations show that the electronic structure of 1T-structure $IrTe_2$ is similar to that of $PdTe_2$, except that the type-II Dirac points lie at 0.18 eV above E_F in $IrTe_2$ (Figs. 1(f) and 1(g)). This is because the number of valence electrons of $IrTe_2$ is one less than that of $PdTe_2$. The calculated three-dimensional (3D) constant energy surface at the energy of the Dirac point in Fig. 1(e) shows that a small electron pocket touches with a large hole pocket at one point, which is an indication of a type-II Dirac point.

Like in other DSMs such as Na_3Bi and Cd_3As_2, the Dirac points in $IrTe_2$ are associated with an inverted band structure. The band inversion in $IrTe_2$ occurs at A point around E_F. With the protection of threefold-rotation symmetry, the band crossing along Γ–A is stabilized, forming the type-II Dirac points. It is thus expected that there are topological surface states (TSSs) in the inverted band gap. Our calculations confirm the existence of TSSs around $\tilde{Z}$ point on (100) surface, as shown in Figs. 1(h) and 1(i). When the Dirac points reside around E_F, the TSSs cross E_F, forming a closed Fermi surface (FS) or a pair of Fermi arcs connecting to the surface projection of the Dirac points.

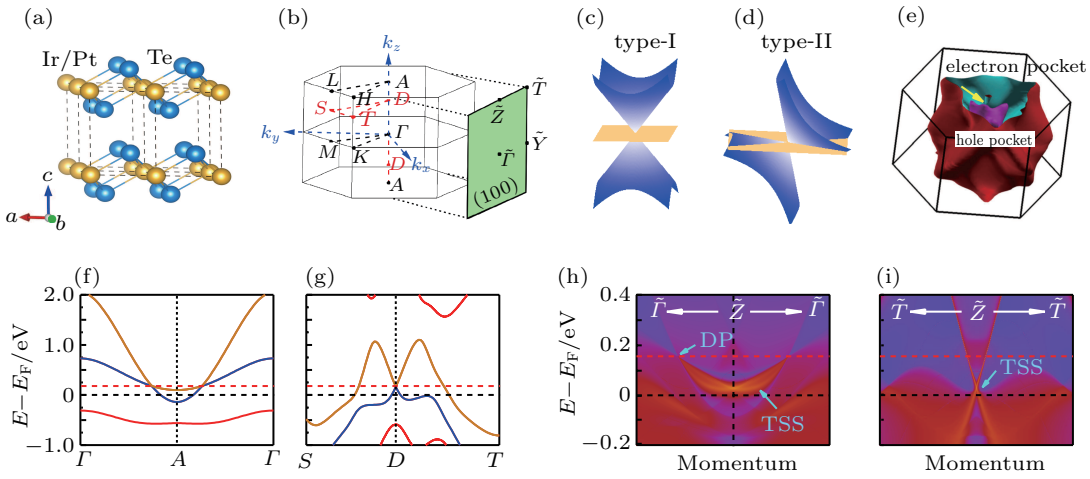

Fig. 1. Crystal structure and calculated electronic structures of $IrTe_2$. (a) Crystal structure. Orange and blue balls represent Ir and Te atoms, respectively. Black dashed lines indicate the unit cells. (b) Bulk BZ and projected (100) surface BZ. Red dots on Γ–A line (labeled as D) mark the momentum locations of the Dirac points (DPs). (c) and (d) Schematic illustrations of type-I and type-II Dirac cones, respectively. (e) Calculated 3D Fermi contours at the energy of the Dirac points. (f) and (g) Calculated bands along Γ–A and S–D–T, respectively, showing the band structures of the type-II Dirac points. (h) and (i) Projection of calculated band dispersions along $\tilde{Z}$–$\tilde{\Gamma}$ and $\tilde{Z}$–$\tilde{T}$, respectively, on (100) surface.

At room temperature, $IrTe_2$ is isostructural to the 1T-structure $PdTe_2$ (Fig. 1(a)) and a structural phase transition occurs at ~ 250 K.[33] By substituting Pt or Pd with Ir, the structural transition is rapidly suppressed, which is accompanied with the appearance of bulk superconductivity.[33] In the phase diagram of $(Ir_{1-x}Pt_x)Te_2$, T_c reaches a maximum of ~ 3 K at $x = 0.05$ and gradually decreases as the Pt content is further increased.[33] We have synthesized a series of $(Ir_{1-x}Pt_x)Te_2$ single crystals with the nominal x up to 0.5. Our resistivity measurements show bulk superconductivity for $x = 0.05$ and 0.1 (Fig. 2(a)). The EDX measurements confirm that the chemical compositions are consistent with the nominal ones (Fig. 2(b)). The variation of Ir and Pt contents is further confirmed by core level photoemission measurements in Fig. 2(d). The x-ray diffraction data recorded on the (001) plane in Fig. 2(c) show a reduction of the c lattice as the Pt content increases. These results clearly indicate variation of the chemical compositions in the series of $(Ir_{1-x}Pt_x)Te_2$ samples that we have synthesized.

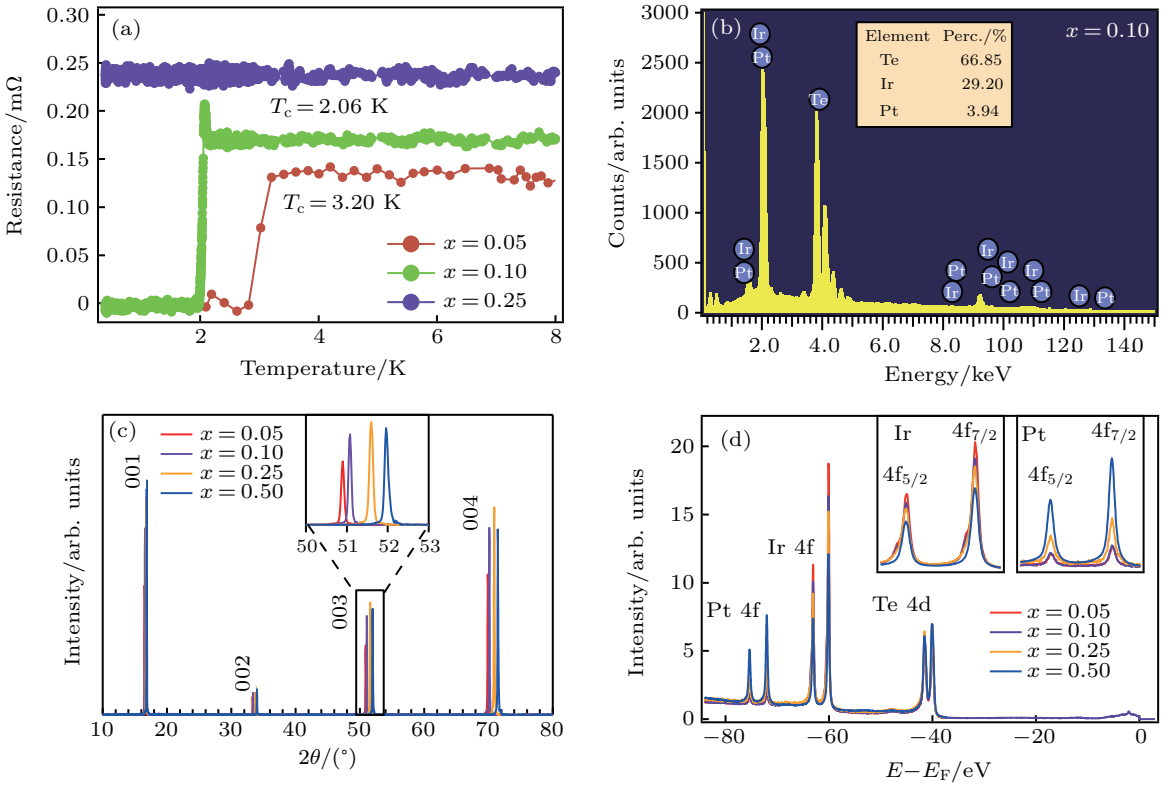

Fig. 2. Superconductivity and chemical compositions of $(Ir_{1-x}Pt_x)Te_2$. (a) Resistivity as a function of temperature for the samples with $x = 0.05$, 0.1, and 0.25. (b) Representative EDX spectrum of one sample with the nominal $x = 0.1$. The inset shows the percentages of Ir, Pt, and Te elements, which are consistent with the nominal composition. (c) XRD data recorded on the (001) plane of single crystals with $x = 0.05$, 0.1, 0.25, and 0.5. Inset shows that the (003) peak position gradually shifts to higher angles as the Pt content increases. (d) Shallow core level spectra of the samples with $x = 0.05$, 0.1, 0.25, and 0.5. The two insets show the evolution of intensities of the Ir 4f and Pt 4f peaks, respectively, with Pt substitution.

Since $IrTe_2$ and $PtTe_2$ have similar electronic structures, in which the Dirac points reside above and below E_F, respectively, the Dirac points can be tuned to E_F in between them. To determine the composition that the Dirac points traverse E_F, we investigate the electronic structures of $(Ir_{1-x}Pt_x)Te_2$ with different doping levels using ARPES.

In Fig. 3, we display the ARPES results of the $x = 0.5$ sample. The calculations indicate that the Dirac point is located on the high-symmetry line Γ–A along the k_z direction. The ARPES experiments were preformed on the (001) cleavage surface. To search for the theoretically predicted Dirac point, we have measured the band structures in the $k_x - k_y$ planes at different k_z values by varying the photon energy $h\nu$ of incident lights, according to the formula $k_z = \sqrt{2m(h\nu - \phi + V_0)}/\hbar$, where ϕ and V_0 are the work function and inner potential, respectively. Figures 3(a) and 3(b) show the ARPES intensity plots and corresponding curvature intensity plots, respectively, along Γ–K direction taken with different photon energies. There is a Dirac-like band crossing at -0.62 eV in all the cuts in Figs. 3(a) and 3(b). The dispersions of the crossing bands do not change as $h\nu$ varies, indicating their surface origin. Notably, there is another Dirac-like band crossing at -0.27 eV in the cut measured at $h\nu = 22$ eV (Figs. 3(a3) and 3(b3)). The crossing bands become separated in the other cuts measured with different $h\nu$ values, indicating that the observed band crossing at -0.27 eV is a 3D Dirac point. The upper branch of the Dirac bands slightly shifts downwards as $h\nu$ increases from 22 eV to 24 eV, but rapidly

moves upwards as $h\nu$ decreases from 22 eV to 20 eV. It seems that the ARPES intensity plot in Fig. 3(a1) at $h\nu = 20$ eV exhibits an outline of an electron-like band below E_F, whereas the maximum intensity appears at E_F. This suggests that the electron-like band is actually located above E_F while the intensity below E_F could arise from a k_z broadening, which is not negligible due to short mean free length of excited photoelectrons. The lower branch of the Dirac bands evolves into a M-shaped band as $h\nu$ increases from 22 eV to 24 eV and a hole-like band as $h\nu$ decreases from 22 eV to 20 eV. As indicated by the guide lines in Fig. 3(a), on the Γ–A line, the bands monotonically shift downwards as $h\nu$ increases from 20 eV to 24 eV, which is consistent with the band calculations in Fig. 3(c). This means that the two crossing bands have the same sign in the slope along the k_z direction, confirming that the Dirac point belongs to the type-II class. In addition to the Dirac band, we observed some other bands that cross E_F at $k_y \sim \pm 0.4$ Å^{-1} in Figs. 3(a) and 3(b). These bands do not change as $h\nu$ varies, and are not consistent with the calculated bulk bands, indicating their surface origin. Figure 3(d) shows the stacking ARPES intensity maps at several constant energies measured at $h\nu = 22$ eV. There is a circular FS around the Brillouin zone (BZ) center at E_F. The FS shrinks into a point at -0.27 eV and then grows into a circle again as the energy is further reduced. These results exhibit that the Dirac cone is nearly isotropic in the k_x–k_y plane. The Dirac point of the $x = 0.5$ sample lies at 0.27 eV below E_F, which is closer to E_F as compared with that in $PtTe_2$, where the Dirac point lies at ~ 1 eV below E_F.[20]

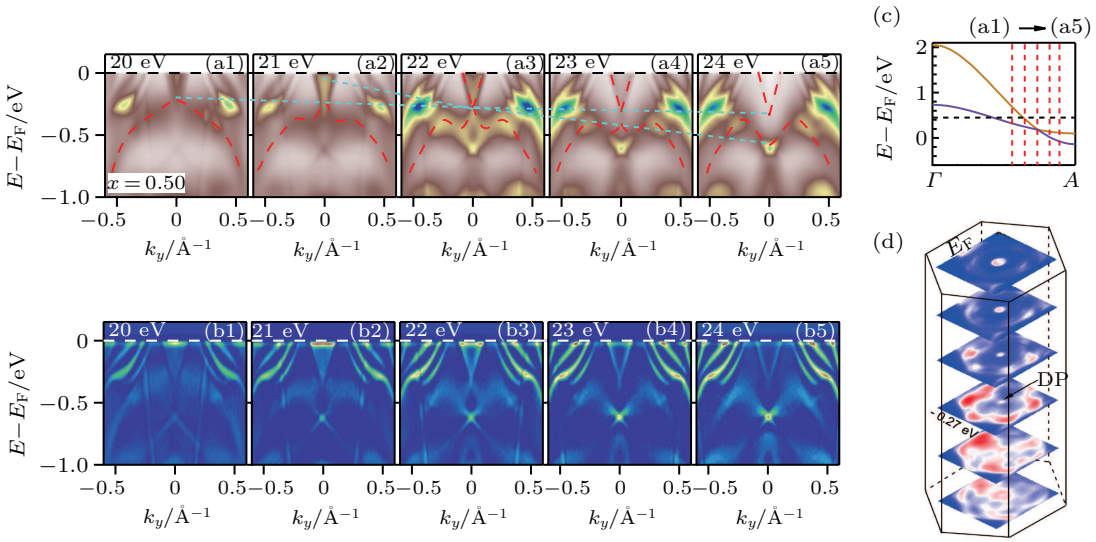

Fig. 3. Electronic structure of the $(Ir_{1-x}Pt_x)Te_2$ sample with $x = 0.5$. (a) ARPES intensity plots along the Γ–K direction measured at (a1) $h\nu = 20$ eV, (a2) 21 eV, (a3) 22 eV, (a4) 23 eV, and (a5) 24 eV. (b) Corresponding curvature intensity plots. (c) Calculated band structure along Γ–A of $IrTe_2$. We determine the chemical potential of $Ir_{0.5}Pt_{0.5}Te_2$ at 0.46 eV, as marked by the horizontal dashed line. The vertical dashed lines indicate the k_z locations of the measured cuts in panels (a) and (b). The inner potential V_0 is set to be 13 eV and the lattice constant c is determined to be 5.27 Å from the XRD data in Fig. 2(c). (d) Stacking plot of the ARPES intensity maps at several constant energies measured at $h\nu = 22$ eV, showing the nearly isotropic Dirac cone structure in the k_x–k_y plane.

Next we focus on the evolution of band structures with the Pt substitution. For all the samples with different Pt contents, the measured band structures are almost consistent except for the energy positions relative to E_F. Figures 4(a)–4(d) show the band dispersions along Γ–K direction measured at $h\nu = 22$ eV for the $(Ir_{1-x}Pt_x)Te_2$ samples with $x = 0.05$, 0.1, 0.25, and 0.5, respectively. The results clearly show that the Dirac point monotonically shifts upwards with the decrease of Pt content. In Fig. 4(g), we extract the Dirac bands from the ARPES data. Figure 4(h) plots the energy position of the Dirac point as a function of Pt content, from which we determine that the Dirac point passes through E_F at $x \sim 0.1$. Figure 4(e) exhibits that two linearly dispersive bands for the $x = 0.1$ sample cross each other at E_F, leading to a point-like FS at the BZ center in Fig. 4(f). Figure 4(h) shows that the Dirac point does not shift linearly with the doping level. The energy shift becomes faster at higher Pt contents. The extrapolation based on the trend is consistent with the previous result in $PtTe_2$.[20] We note that if the calculated bands of $IrTe_2$ are rigidly shifted, the Dirac point would pass through E_F around $x = 0.25$. This value is higher than that determined from our experimental results. This might be because the band calculations slightly overestimate the energy of the Dirac point in $IrTe_2$. The previous study in $PtTe_2$ shows similar inconsistency between calculation and experiment,[20] with a discrepancy of ~ 0.1 eV.

The substitution of Pt in $IrTe_2$ not only raises the chemical potential, making the type-II Dirac points approach E_F, but also introduces bulk superconductivity into the system. The maximum T_c is up to ~ 3 K, which is accessible in many experimental techniques, making it possible to study the physical

properties of Dirac fermions in the superconducting state. The theoretical studies have proposed that topological superconductivity could be realized in type-I DSMs.[14,15] In contrast, there is no theoretical study on the superconducting properties of type-II DSMs. Moreover, as the Dirac points are close to E_F in the superconducting $(Ir_{1-x}Pr_x)Te_2$, the associated topological surface bands may cross E_F, forming a pair of Fermi arcs or a closed FS. The proximity effect induces superconductivity in the TSSs below T_c, which could realize two-dimensional topological superconductivity on the surface of DSMs, in analogy to that in superconducting topological insulators. Our results suggest that the Pt-substituted $IrTe_2$ would be a promising material for studying the topological superconductivity of bulk and surface states in DSMs, and may find potential application in novel quantum devices such as quantum computers.

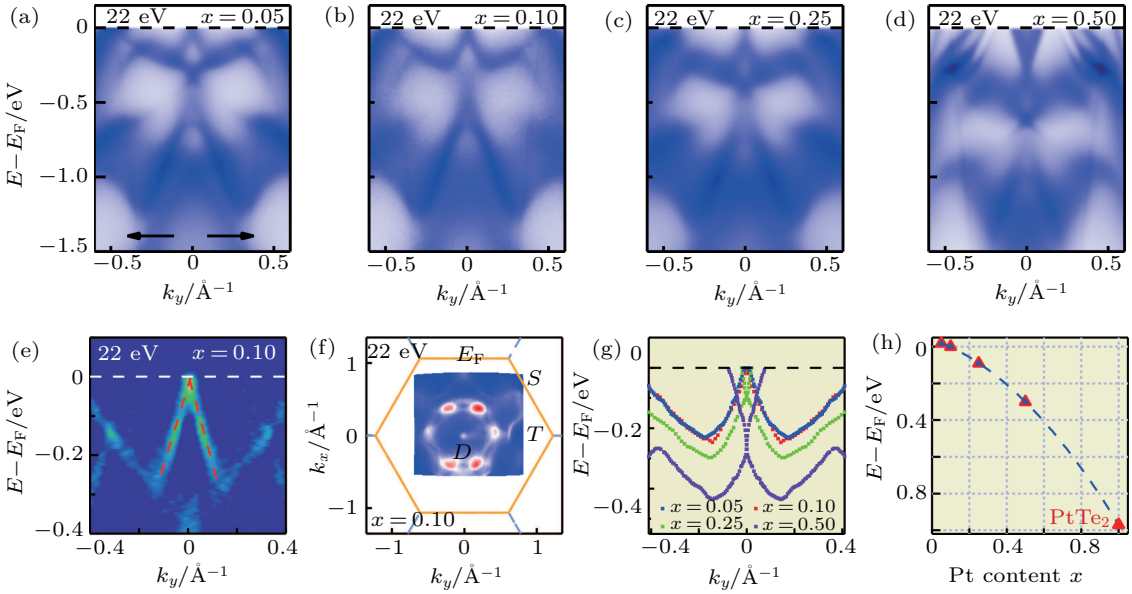

Fig. 4. Evolution of the Dirac point with Pt substitution. (a)–(d) Band dispersions along the Γ–K direction measured at $h\nu = 22$ eV for the $(Ir_{1-x}Pt_x)Te_2$ samples with $x = 0.05$, 0.1, 0.25, and 0.5, respectively. (e) Second derivative intensity plot of the data in panel (b), showing the Dirac point lying at E_F for the $x = 0.1$ sample. Dashed lines are guide to the eye, indicating the linear Dirac bands. (f) ARPES intensity map at E_F measured at $h\nu = 22$ eV for the $x = 0.1$ sample, showing the point-like FS at the BZ center. (g) Extracted Dirac bands from the data in panels (a) to (d). (h) Energy of the Dirac point as a function of the Pt content. The energy for $PtTe_2$ is extracted from the previous result in Ref. [20].

Acknowledgment

We thank Chen Fang for the discussion. Y.B.H. acknowledges support by the Chinese Academy of Sciences (CAS) Pioneer "Hundred Talents Program" (type C).

References

[1] Qi X L and Zhang S C 2011 *Rev. Mod. Phys.* **83** 1057
[2] Hasan M Z and Kane C L 2010 *Rev. Mod. Phys.* **82** 3045
[3] Hor Y S, Williams A J, Checkelsky J G, Roushan P, Seo J, Xu Q, Zandbergen H W, Yazdani A, Ong N P and Cava R J 2010 *Phys. Rev. Lett.* **104** 057001
[4] Zhang J L, Zhang S J, Weng H M, Zhang W, Yang L X, Liu Q Q, Feng S M, Wang X C, Yu R C, Cao L Z, Wang L, Yang W G, Liu H Z, Zhao W Y, Zhang S C, Dai X, Fang Z and Jin C Q 2011 *Proc. Natl. Acad. Sci. USA* **108** 24
[5] Wang M X, Liu C H, Xu J P, Yang F, Miao L, Yao M Y, Gao C L, Shen C Y, Ma X C, Chen X, Xu Z A, Liu Y, Zhang S C, Qian D, Jia J F and Xue Q K 2012 *Science* **336** 52
[6] Sasaki S, Ren Z, Taskin A A, Segawa K, Fu L and Ando Y 2012 *Phys. Rev. Lett.* **109** 217004
[7] Chadov S, Qi X L, Kubler J, Fecher G H, Felser C and Zhang S C 2010 *Nat. Mater.* **9** 541
[8] Lin H, Wray L A, Xia Y Q, Xu S Y, Jia S, Cava R J, Bansil A and Hasan M Z 2010 *Nat. Mater.* **9** 546
[9] Liu C, Lee Y, Kondo T, Mun E D, Caudle M, Harmon B N, Bud'ko S L, Canfield P C and Kaminski A 2011 *Phys. Rev. B* **83** 205133
[10] Liu Z K, Yang L X, Wu S C, Shekhar C, Jiang J, Yang H F, Zhang Y, Mo S K, Hussain Z, Yan B, Felser C and Chen Y L 2016 *Nat. Commun.* **7** 12924
[11] Sakano M, Okawa K, Kanou M, Sanjo H, Okuda T, Sasagawa T and Ishizaka K 2015 *Nat. Commun.* **6** 8595
[12] Zhang P, Yaji K, Hashimoto T, Ota Y, Kondo T, Okazaki K, Wang Z J, Wen J S, Gu G D, Ding H and Shin S 2018 *Science* **360** 182
[13] Wang D F, Kong L Y, Fan P, Chen H, Zhu S Y, Liu W Y, Cao L, Sun Y J, Du S X, Schneeloch J, Zhong R D, Gu G D, Fu F, Ding H and Gao H J 2018 *Science* **362** 333
[14] Kobayashi S and Sato M 2015 *Phys. Rev. Lett.* **115** 187001
[15] Hashimoto T, Kobayashi S, Tanaka Y and Sato M 2016 *Phys. Rev. B* **94** 014510
[16] Hosur P, Dai X, Fang Z and Qi X L 2014 *Phys. Rev. B* **90** 045130
[17] Aggarwal L, Gaurav A, Thakur G S, Haque Z, Ganguli A K and Sheet G 2016 *Nat. Mater.* **15** 32
[18] Wang H, Wang H C, Liu H W, Lu H, Yang W H, Jia S, Liu X J, Xie X C, Wei J and Wang J 2016 *Nat. Mater.* **15** 38
[19] He L P, Jia Y T, Zhang S J, Hong X C, Jin C Q and Li S Y 2016 *Npj Quant. Mat.* **1** 16014
[20] Yan M Z, Huang H Q, Zhang K N, Wang E Y, Yao W, Deng K, Wan G L, Zhang H Y, Arita M, Yang H T, Sun Z, Yao H, Wu Y, Fan S S, Duan W H and Zhou S Y 2017 *Nat. Commun.* **8** 257
[21] Fei F C, Bo X Y, Wang R, Wu B, Jiang J, Fu D Z, Gao M, Zheng H, Chen Y L, Wang X F, Bu H J, Song F Q, Wan X G, Wang B G and Wang G H 2017 *Phys. Rev. B* **96** 041201
[22] Noh H J, Jeong J, Cho E J, Kim K, Min B I and Park B G 2017 *Phys. Rev. Lett.* **119** 016401

[23] Zhang K N, Yan M Z, Zhang H X, Huang H Q, Arita M, Sun Z, Duan W H, Wu Y and Zhou S Y 2017 *Phys. Rev. B* **96** 125102
[24] Wang Z J, Sun Y, Chen X Q, Franchini C, Xu G, Weng H M, Dai X and Fang Z 2012 *Phys. Rev. B* **85** 195320
[25] Liu Z K, Zhou B, Zhang Y, Wang Z J, Weng H M, Prabhakaran D, Mo S K, Shen Z X, Fang Z, Dai X, Hussain Z and Chen Y L 2014 *Science* **343** 864
[26] Wang Z J, Weng H M, Wu Q S, Dai X and Fang Z 2013 *Phys. Rev. B* **88** 125427
[27] Liu Z K, Jiang J, Zhou B, Wang Z J, Zhang Y, Weng H M, Prabhakaran D, Mo S K, Peng H, Dudin P, Kim T, Hoesch M, Fang Z, Dai X, Shen Z X, Feng D L, Hussain Z and Chen Y L 2014 *Nat. Mater.* **13** 677
[28] Soluyanov A A, Gresch D, Wang Z J, Wu Q S, Troyer M, Dai X and Bernevig B A 2015 *Nature* **527** 495
[29] Deng K, Wan G L, Deng P, Zhang K N, Ding S J, Wang E Y, Yan M Z, Huang H Q, Zhang H Y, Xu Z L, Denlinger J, Fedorov A, Yang H T, Duan W H, Yao H, Wu Y, Fan S S, Zhang H J, Chen X and Zhou S Y 2016 *Nat. Phys.* **12** 1105
[30] Huang L, McCormick T M, Ochi M, Zhao Z Y, Suzuki M T, Arita R, Wu Y, Mou D X, Cao H B, Yan J Q, Trivedi N and Kaminski A 2016 *Nat. Mater.* **15** 1155
[31] Fei F C, Bo X Y, Wang P D, Ying J H, Li J, Chen K, Dai Q, Chen B, Sun Z, Zhang M H, Qu F M, Zhang Y, Wang Q H, Wang X F, Cao L, Bu H J, Song F Q, Wan X G and Wang B G 2018 *Adv. Mater.* **30** 1801556
[32] Kresse G and Hafner J 1993 *Phys. Rev. B* **48** 13115
[33] Yang J J, Choi Y J, Oh Y S, Hogan A, Horibe Y, Kim K, Min B I and Cheong S W 2012 *Phys. Rev. Lett.* **108** 116402